Arab J Geosci
DOI 10.1007/s12517-010-0226-y

ORIGINAL PAPER

3D geomodeling of the Lower Cretaceous oil reservoir, Masila oil field, Yemen

Hassan S. Naji · Mohammed Khalil Khalil

Received: 29 January 2010 / Accepted: 19 October 2010

Abstract Oil was first discovered in the Masila area of Yemen in the late 1990s, with about 90% of the reserves found in the Lower Qishn Clastic Member of the Qishn Formation. The porosity determinations of the Lower Qishn Clastic are relatively high and the permeability ranges from 103 to 374 md. This paper tries to evaluate the hydrocarbons in the porous zones encountered in the Lower Cretaceous formations, which were penetrated by the eight wells in the study area. The water saturation shows low values, while the hydrocarbon saturation is in a reverse relation, i.e., the hydrocarbon increases where the water saturation decreases. Different cross-plots such as Rho-PHIN, Rho-DTN, and M-N were used in lithological identification for the two studied formations (Saar and Qishn) in the studied wells. Formation evaluation and presentation forms of the obtained petrophysical parameters have frequently proven that the formations have high hydrocarbon saturation in this area and contain many pay zones. On of the main targets of this paper is to build a detailed 3D geological modeling of the Lower Cretaceous Sequence conducted through an integrated study.

Keywords 3D geomodeling · Oil potentialities · Lower Cretaceous · Oil pay zone · History matching

H. S. Naji · M. K. Khalil (✉)
Department of Petroleum Geology and Sedimentology, Faculty of Earth Sciences, King Abdelaziz University,
Jeddah, Saudi Arabia
e-mail: mazenkhalil2006@yahoo.com

H. S. Naji
e-mail: hnaji@kau.edu.sa

Introduction

Oil was first discovered in the Masila area (Fig. 1) in the late 1990s, with commerciality being declared in late 1991 and oil production commenced in July 1993. By the end of December 1999, the total known oil-in-place exceeds 1.6 billion stock tank barrels (STB), with proven ultimate recoverable oil reserves approaching 900 million STB. The Qishn Formation was deposited as predominantly post-rift sediments in the east/west-oriented Say'un–al Masila rift basin that initiated during Late Jurassic to Early Cretaceous as part of the second Mesozoic rift phase. Deposition was related to a regional east to west transgression overlying a regional lower Cretaceous unconformity at the top of the Sa'af Member. Regionally, the Qishn Formation was deposited on an inner neritic to shallow-marine platform setting within the graben. During deposition of the Qishn Formation, the Say'un–Masila Basin was open to fully marine waters based on the presence of correlative carbonate strata toward the southeast at Socotra Island in the Gulf of Aden. Carbonates intertongue with fluvial deltaic to littoral deposits, becoming fully siliciclastic westwards. The Barremian to Aptian age range for the Qishn Formation was confirmed by samples analyzed in 1994. The Qishn Formation is likely to be equivalent to the lower fluviatile sandstones of the Tawilah Group of western Yemen, and to the east, it becomes more carbonate-rich and passes into the purer carbonate facies of the Mahra Group (Fig. 2b). In the Masila area, the Lower Cretaceous sequence is divided, from base to top, into Saar and Qishn Formations.

The integration of geological and geophysical data leads to better reservoir characterization (Naji and Khalil 2010; Khalil and Naji 2010; Greenwood 1967; Greenwood and Bleackley 1967; Naji 2010; Naji et al. 2010a, b).

Published online: 16 November 2010

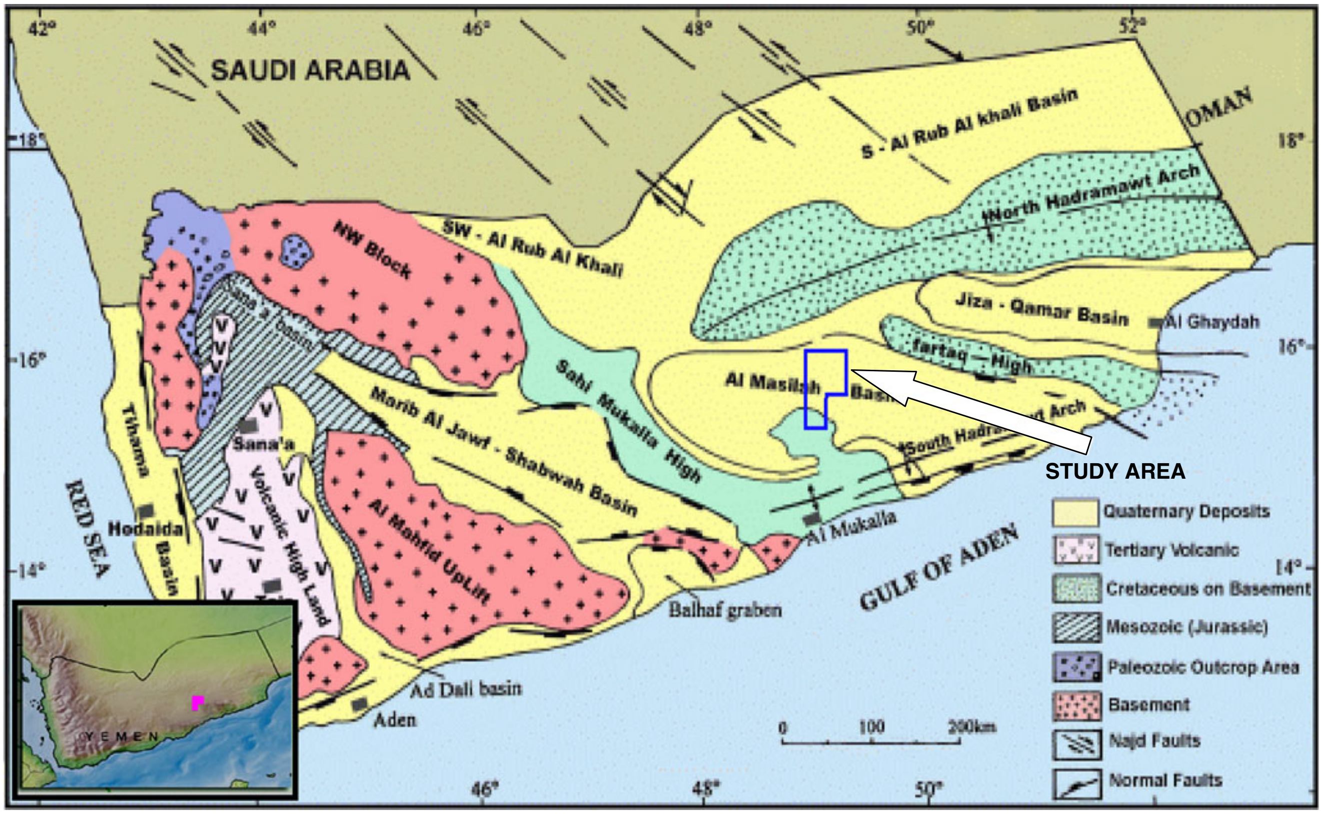

Fig. 1 Geological map of Yemen with location of the study area and principal sedimentary basins (modified from Beydoun et al. 1998)

Stratigraphic setting

Figure 2a (Canadian Oxy Company 2003) shows the general stratigraphy of the study area, from oldest to youngest, as follows.

Precambrian

The upper part of basement of the Say'un–Masila Basin consists mostly of metamorphosed Precambrian to Lower Cambrian sediments (Fig. 1). It is unconformably overlain by Middle to Upper Jurassic sequence.

Kohlan Formation

During the Middle–Late Jurassic, sandstones were deposited widely across the area now occupied by Yemen, with thick sedimentation within depositional lows of pre-Jurassic topography. These thick sandstone deposits are known as the Kohlan Formation (Fig. 2a) and include siltstone, sandstone, and conglomerate with thin limestones and green clay.

Shuqra Formation

The Shuqra Formation (Fig. 2a) is generally composed of lime mudstones, wackestones, and grainstones. The Shuqra Formation is of Upper Jurassic age (Oxfordian to Kimmeridgian) and forms carbonate platform with reefal buildups.

Madbi Formation

The Madbi Formation consists of porous lime grainstone to argillaceous lime mudstone (Fig. 2a), of which the lithofacies represents deposition within an open marine environment. This unit is classified into two members. The lower member is commonly made up of argillaceous limestones and sandstones and forms a good reservoir in some oil fields of the Masila Basin (Canadian Oxy Company 2003). The upper member is composed of laminated organic-rich shale, mudstone, and calcareous sandstone and is a prolific source rock in the Masila province (Mills 1992).

Naifa Formation

In general, the Naifa Formation is composed mainly of silty and dolomitic limestone and lime mudstone with wackestone and chalk (Fig. 2a). The upper part of the formation is composed of very porous clastic carbonates overlain by the Saar dolomite facies. The Formation was deposited as chalk and lime mudstones in shallow water to deepwater marine conditions.

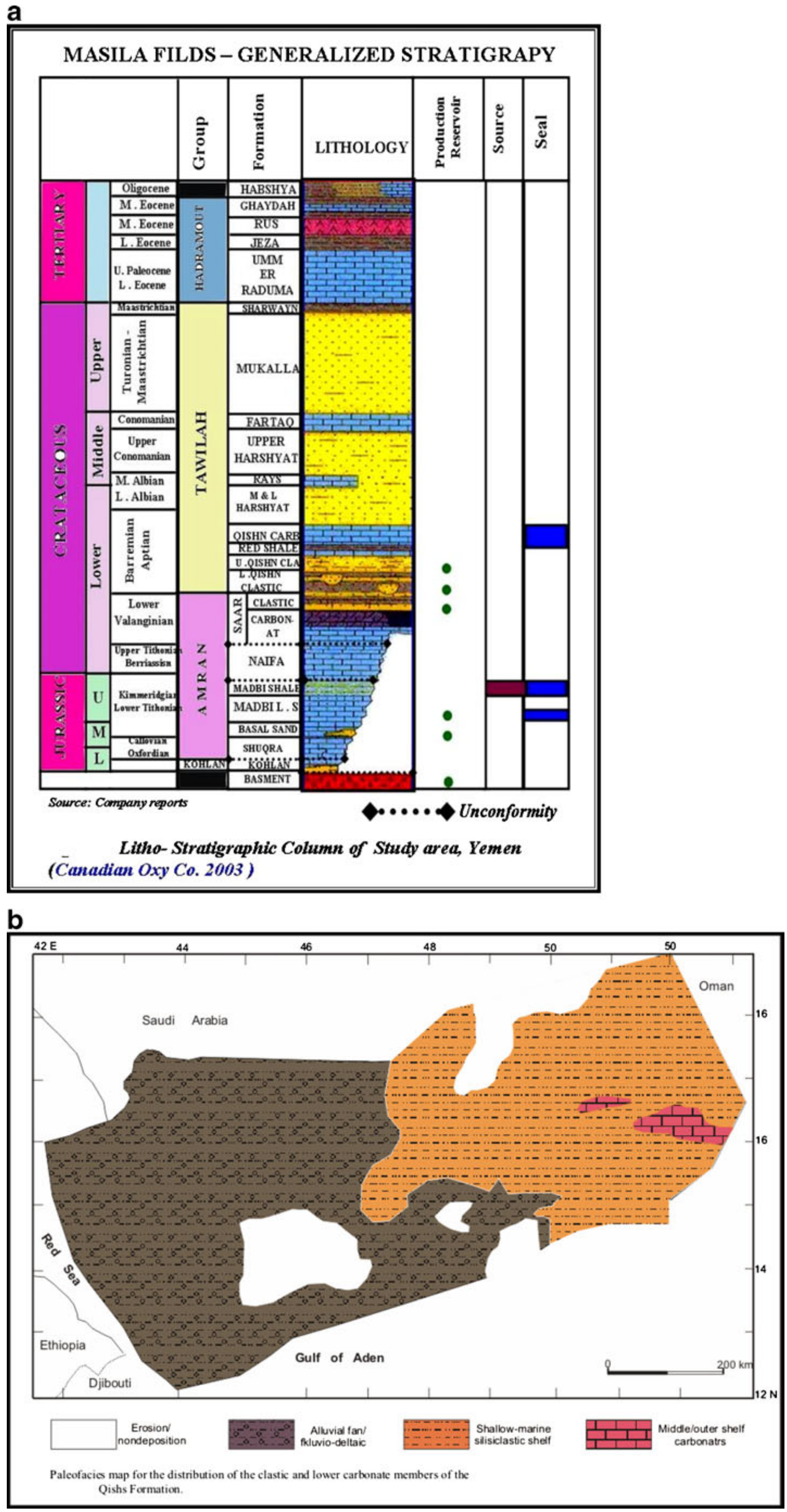

Fig. 2 **a** Lithostratigraphic column and oil potentialities of Masila oil field. **b** Facies map for the Clastic and Lower Carbonate members of the Qishn Fm

Saar Formation

This formation overlies the Naifa Formation and is composed mainly of limestone, with some mudstone and sandstones (Fig. 2a). Oil companies classified the formation into lower Saar carbonates and upper Saar clastics.

Qishn Formation

The term "Qishn Formation" was first defined by Beydoun (1964) and further refined in Beydoun (1966) and Beydoun and Greenwood (1968) and is used widely by operating oil companies in Yemen. The Qishn Formation could be divided into four easily separated members as follows. The lowest two members of the Qishn Formation are the laterally equivalent to the Clastic Member and the Lower Carbonate Member. All the members pass laterally into a clastic-dominated section in western Yemen (Holden and Kerr 1997). The upper member (Carbonate Member) is composed of limestone with subordinate dolomites (Fig. 2a). Under the Carbonate Member, there is a widespread mudstone unit, called the Shale Member (Fig. 3).

Late Lower Cretaceous–Tertiary formations

The Late Lower Cretaceous–Tertiary formations consist of Harshiyat Formation (clastics) and Fartaq Formation (carbonate), Mukalla Formation (Coniacian though Campanian—fluvial sediments, Fig. 2a), Sharwan Formation (Mastrichtian—carbonates), Umm Er-Radhuma Formation (dominantly carbonates, Paleocene Early Eocene), Rus Formation (Middle Miocene—anhydrites, Fig. 2a), Ghaydah Formation (Middle to Late Eocene—carbonate), and shallow marine fine-grained Clastics of the Habashiya Formation.

a

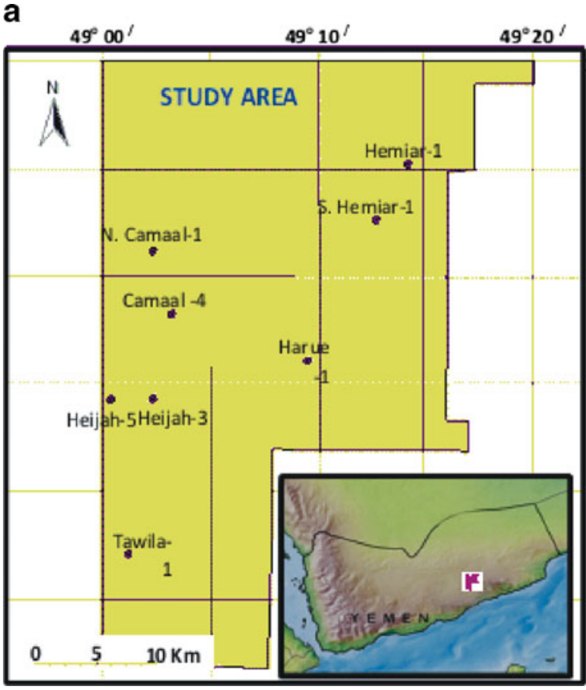

Fig. 3 **a** Location map showing the study wells in Masila oil field. **b** Sample for the available well log data plot output

Materials and methods

Well logs data methodology

Eight wells, which cover the whole study area, were selected based on the different log types (Fig. 4). The available well logs are listed in Table 1. These logs include: gamma ray (GR), caliper, spontaneous potential (SP), apparent formation resistivity (R_{wa}), micro-spherically focused log (MSFL), laterolog shallow and deep (LLS and LLD), formation density compensated, borehole compensated sonic, compensated neutron log (CNL), and litho-density tool. These logs are checked and matched for depth before processing and interpretation.

A detailed foot-by-foot analysis was required to allow summations of reservoir properties over each of the many stratigraphic horizons. The well log evaluation has been achieved using PC-based software application for reservoir property analysis and summation.

Shale volume (V_{sh}) was calculated from single curve indicators, such as the GR, SP, and deep resistivity (RESD) responses, and double curve indictors. The minimum of these values at each level was selected as the final value for shale volume. A unique clean sand and pure shale value for GR, SP, and RESD were chosen for each zone in each well. A linear relationship was applied to the V_{sh} from GR. The resistivity equation for V_{sh} is similar to the GR equation, but using the logarithm of resistivity in each variable.

Where a full suite of porosity logs was available, the effective porosity (PHIe) was based on a shale-corrected complex lithology model using PEF, density, and neutron data. This method is quite reliable in a wide variety of rock types. No matrix parameters are needed by this model, unless light hydrocarbons are present. Shale-corrected density and neutron data are used as inputs to the model. Results were depending on shale volume and the density and neutron shale properties selected for the calculation. In wells with an incomplete suite of porosity logs, the shale-corrected density log, shale-corrected neutron log, or the shale-corrected sonic log have been used to build the model.

The equation used was $PHIe = PHIt \times (1 - V_{sh})$. This step was the most important contribution to the project as it

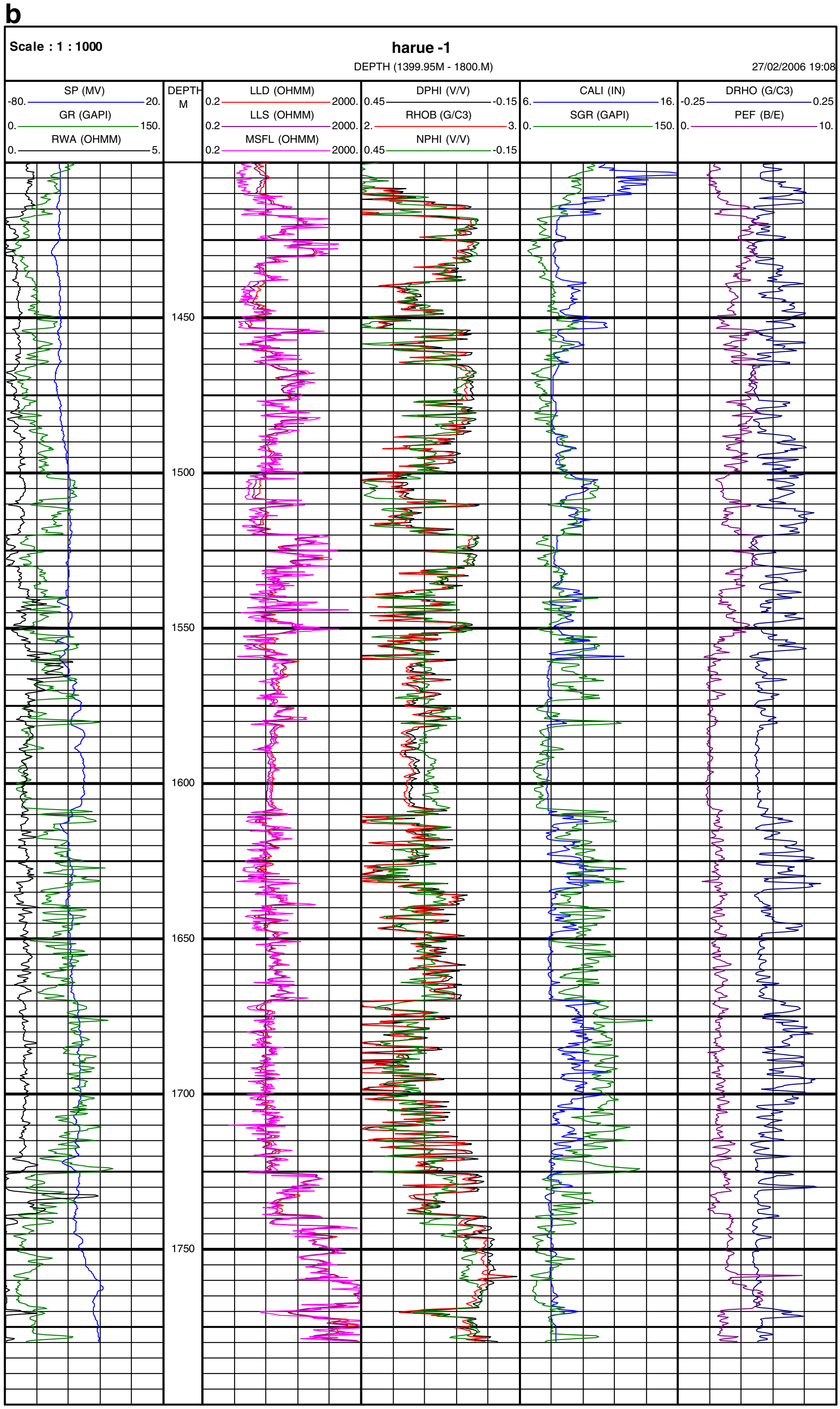

Fig. 3 (continued)

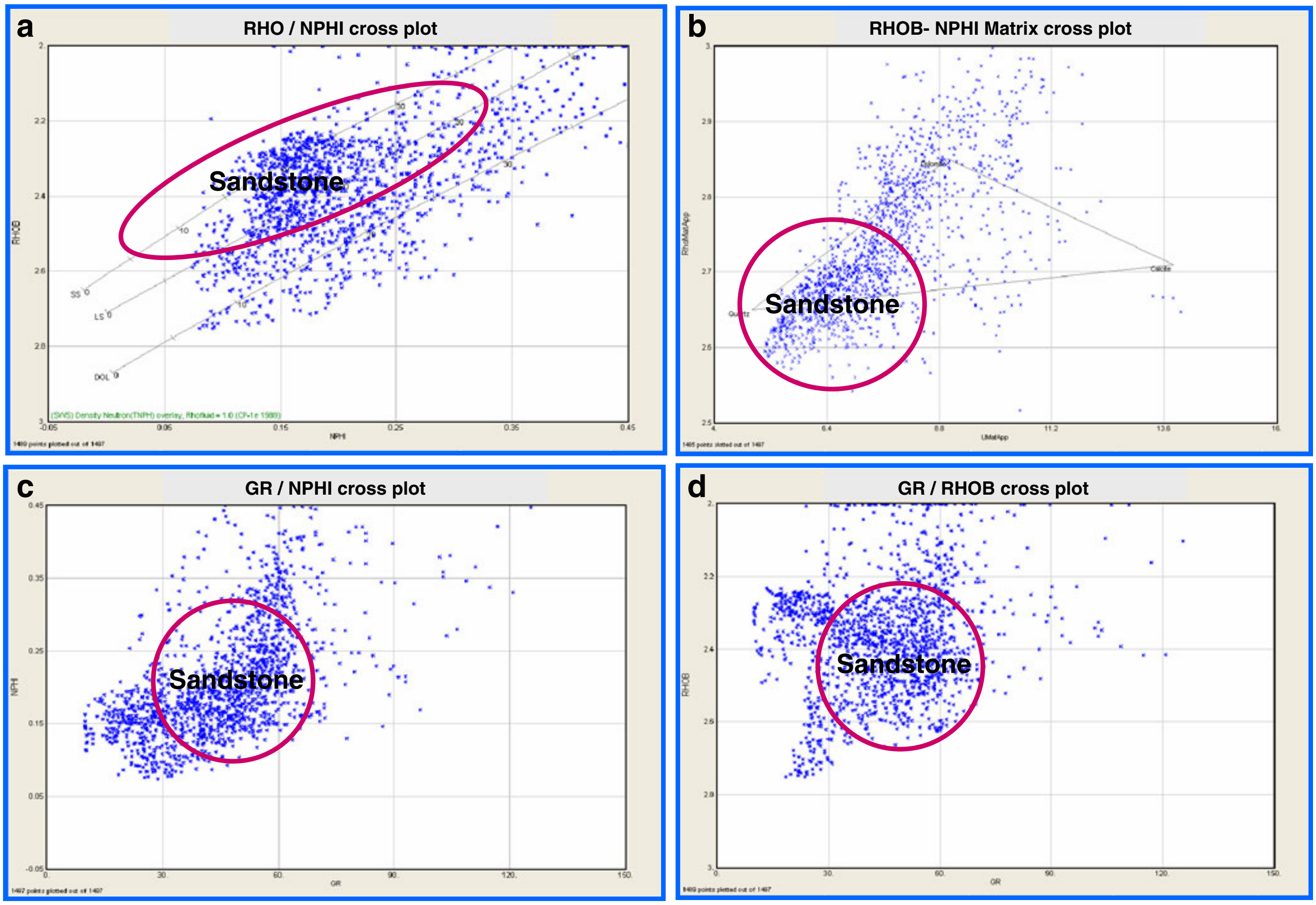

Fig. 4 Lithological identification cross-plots of Lower Qishn Clastic–North Camaal-1 well

integrates all available data in all wells in a consistent manner. The value for total porosity, PHIt, was derived from combining the readings of two porosity logs of the density and neutron logs.

After that, both old and new wells were treated identically, with water saturation, permeability, and mappable reservoir properties being derived in a uniform and consistent manner.

Water saturation (S_w) was computed with a shale correction using the Simandoux equation and the Waxman–Smits equation (Rojstaczer et al. 2008). Both equations reduce to the Archie equation when shale volume is zero. Simandoux and Waxman–Smits methods gave very similar results in this project area. The resistivity curves used were the long normal from ES logs, the deep induction, or the deep laterolog.

Absolute permeability at each well of the study area is estimated using the following relation (Rojstaczer et al. 2008):

$$\log K = \frac{\ln(\varphi_e(1 - S_{wi})}{0.59} + 5.0$$

Table 1 Available open hole well logs in the study area

No.	Well name	Available data
1	Camaal-4	GR, SP, LLS, LLD, MSFL, DTLN, RWA, CAL, PEF, RHOB, DRHO, NPHI, DPHI, SGR
2	Haru-1	GR, LLS, LLD, MSFL, RWA, CAL, SP, PEF, RHOB, DRHO, NPHI, DPHI, SGR
3	Heijah-3	GR, LLS, LLD, MSFL, DTLN, RWA, SP, CAL, PEF, DRHO, RHOB, NPHI, DPHI, SGR
4	Heijah-5	RWA, CAL, GR, SP, LLS, LLD, MSFL, SGR, PEF, DRHO, RHOB, NHPI, DPHI
5	Hemiar-1	CAL,GR, SP, LLS, LLD, MSFL, RWA, SGR, PEF, DRHO, PEF, RHOB, NPHI, DPHI
6	South Hemiar-1	RWA,GR, SP, LLS, LLD, MSFL, CAL, DTLN, SGR, PEF, DRHO, NPHI, DPHI, RHOB
7	North Camaal-1	GR, RWA, SP, LLD, LLS, MSFL, DTLN, CAL, SGR, PEF, RHOB, DRHO, NPHI, DPHI
8	Tawila-1	GR, SP, RWA, LLS, LLD, MSFL, CAL, DTLN, SGR, DRHO, PEF, RHOB, NPHI

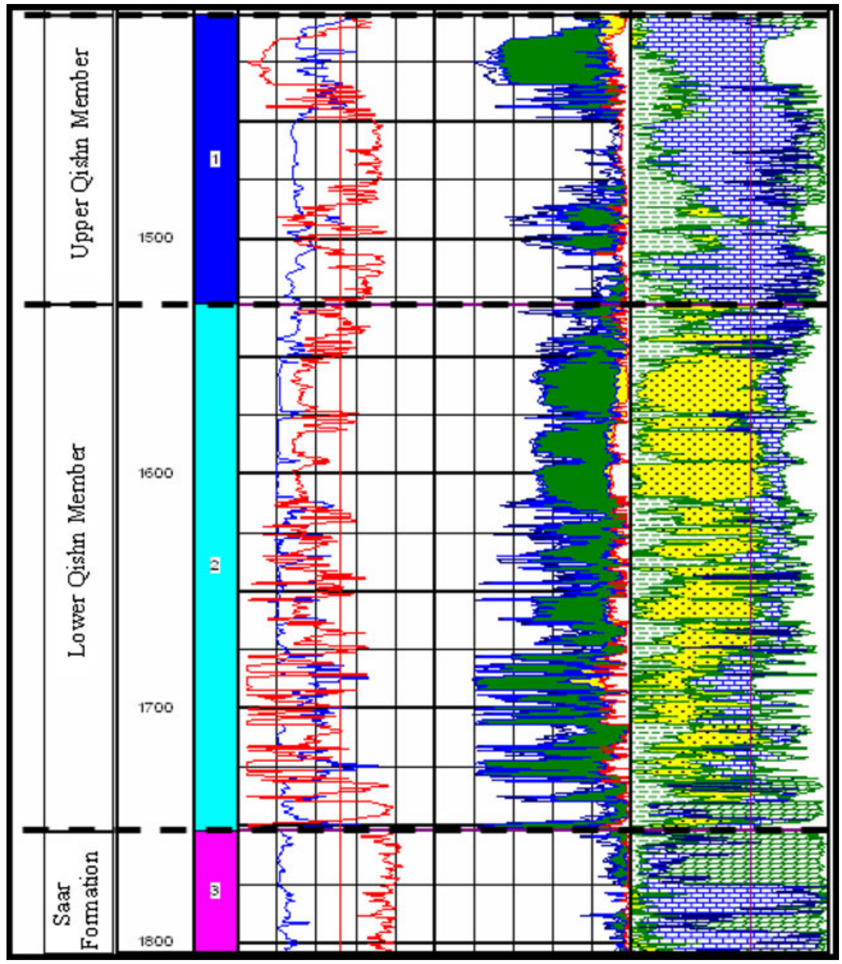

Fig. 5 Masila oil field reservoirs including Saar Formation and Lower Qishn and Upper Qishn members

where K is the absolute permeability in millidarcies, φ_e is the effective porosity, and S_{wi} is the irreducible water saturation.

Porosity values were distributed across the model using sequential Gaussian simulation (SGS). Similarly, water saturation and permeability were distributed with SGS collocated on the distributed porosity data.

Water saturation calculations are based on the distributions related to porosity ranges. This fast and simple method allows the generation of a consistent water saturation distribution that respects a realistic degree of correlation between porosity and saturation.

Sequential indicator simulation method was chosen to distribute three facies types in each reservoir interval—shale, sandstone facies, and carbonates facies—using the flags created in petrophysical information (Fig. 5). Reservoir properties, such as initial water saturations, porosities, permeabilities, and facies, were upscaled into model cells along the well paths from processed well logs.

3D geomodeling data and methodology

One of the main aspects of building the proposed 3D model is to understand the data and check the quality of the data

Table 2 Available data of the most important aspects of building any 3D model

Data	Formats	Type
Well data		
Well headers	(Well heads (*.*))	Well
Well deviations	(well path deviation)(ASCII)(*.*)	Well
Well logs	(Well log (LAS 3.0) (*.las)	Well
Well tops	(ASCII) (*.*)	Well tops
3D seismic data	Seisworks Horizon Pick (ASCII) (*.*)	Lines

PHT total porosity, *PHE* effective porosity, R_w water resistivity, S_w water saturation files (Table 2). Extensive data sets were used to construct the geological model of the reservoir such as:

1. Geological structures (major horizons, permeability barriers, fluid contacts, etc.).
2. Fault polygons for all major faults
3. Processed log data for eight well penetrations.
4. Well log data (porosity, permeability, saturations, etc.).
5. Seismic data.

1. Well data

   Wells data are imported in three steps:

   (a) Well head data: A well head file was created to specify the top position of the well and length of the well path.
   (b) Well path/deviation data
   (c) Well log data: Several well logs for eight wells (Table 1), which cover the whole study area, were selected (petrophysical parameters logs in LAS format).
2. Well tops data

   A table with ASCII format for the tops of the studied horizons has been used.
3. Seismic data

   The available seismic data include seismic horizons for top upper Qishn, top lower Qishn, top Saar, and top Basement in addition to fault polygons.

Procedure for building the 3D geological modeling

The processes of building 3D geological models are:

(a) Creating geological and geophysical modeling to construct the geological framework for the studies reservoir
(b) Reservoir characterization–distribution of the geological rock units, facies, and fluid properties
(c) Reservoir flow modeling through upscaling (or upgridding) and flow modeling

A set of equations was derived from well tests and porosity logs and used to populate the 3D grid. This method for deriving permeability distribution gives satisfactory results.

Results and discussion

Cross-plot lithological identification

The type and amount of each lithologic component for Lower Qishn Clastic was determined through different cross-plots. These cross-plots give a quick view about the rock and mineral contents in a qualitative way. Some of these cross-plots give the amount of lithologic contents in a quantitative way. These cross-plots include the NPHI-RHOB cross-plot, NPHI-RHOB matrix cross-plots, and GR-RHOB GR-NPHI cross-plots. It is clear that the lithology for all wells is almost the same. The lithological identification of North Camaal-1 well is an example of such cross-plots (Fig. 4a–d).

RHOB/NPHI cross-plot identification

The cross-plot of RHOB/NPHI (Fig. 4a) shows that the main lithology is carbonates (limestone and dolomite) with shale for the Lower Qishn Clastic rock unit. The sandstone content is generally low, as shown from the lesser plotted points along the sandstone line.

Table 3 PHT, PHE, R_w, S_w, and hydrocarbon saturation of the Saar Fm and the Qishn units in the study wells

Parameters	Formation	Heijah-5 (%)	Heijah-3 (%)	N.Camaal- 1 (%)	Camaal-4 (%)	Harue-1 (%)	S. Hemiar-1 (%)	Hemiar-1 (%)	Tawila-1 (%)
Total porosity	Upper Qishn Carb.	17.7	20.7	18.2	20.7	14.3	14.6	14.9	16.4
	Lower Qishn clastic	20.9	24.9	19.7	21.7	21.6	22.8	22.7	20.8
	Saar Formation	19.7	16.3	19.4	10.6	5.23	11	10.4	9.2
Effect porosity	Upper Qishn Carb.	12.2	14.3	16.1	18.9	10.6	13.9	10.8	14.5
	Lower Qishn clastic	17.5	23.7	18.2	21.4	16.8	22.1	18.8	20.4
	Saar Formation	2.88	9.3	18.2	8	5.21	6.7	5.7	8.6
Water resistivity	Upper Qishn Carb.	0.62	0.55	0.77	1.90	0.50	0.61	0.89	0.91
	Lower Qishn clastic	2.03	1.89	2.60	2.50	1.29	1.58	2.50	1.67
	Saar Formation	0.312	0.22	0.64	0.48	0.61	0.95	0.41	0.64
Water saturation	Upper Qishn Carb.	60.6	65.1	54.3	48.2	62.3	57.9	58.9	55.7
	Lower Qishn clastic	31.6	32.6	28.8	30.9	31.8	31.4	29.9	37.2
	Saar Formation	75.4	80.2	69.6	67.5	75.6	61.3	67.00	53.3
Hydrocarbon saturation (Sh)	Upper Qishn Carb.	39.4	34.9	45.7	51.8	37.7	42.1	41.1	44.3
	Lower Qishn clastic	68.4	67.4	71.2	69.1	68.16	68.6	70.1	62.8
	Saar Formation	24.6	19.8	30.4	32.5	24.4	38.7	33	46.7

RHOB/NPHI matrix cross-plot identification

The cross-plot of RHOB/NPHI matrix (Fig. 4b) reflects the same picture of the above plot. The scattered plotted points show that the main lithology is carbonates (limestone and dolomite) with some shale for the Lower Qishn Clastic rock unit. The sandstone content is low, as shown from the lesser plotted points in the quartz matrix zone.

GR/NPHI cross-plot identification

This plot (Fig. 4c) shows that the plotted points are scattered. This reflects the variation of lithology of the Lower Qishn Clastic rock unit. It shows that the points have a low GR and low NPHI, which indicate the presence of limestone and dolomite. The points with medium GR and medium NPHI indicate sandstone, and the points with high GR and high NPHI reflect the abundance of shale. By comparing, it is clear that the main lithology is limestone and dolomite with shale and a little sandstone.

GR/RHOB cross-plot identification

This plot (Fig. 4d) illustrates the same result as in the above plot, as expected from the density of the limestone and

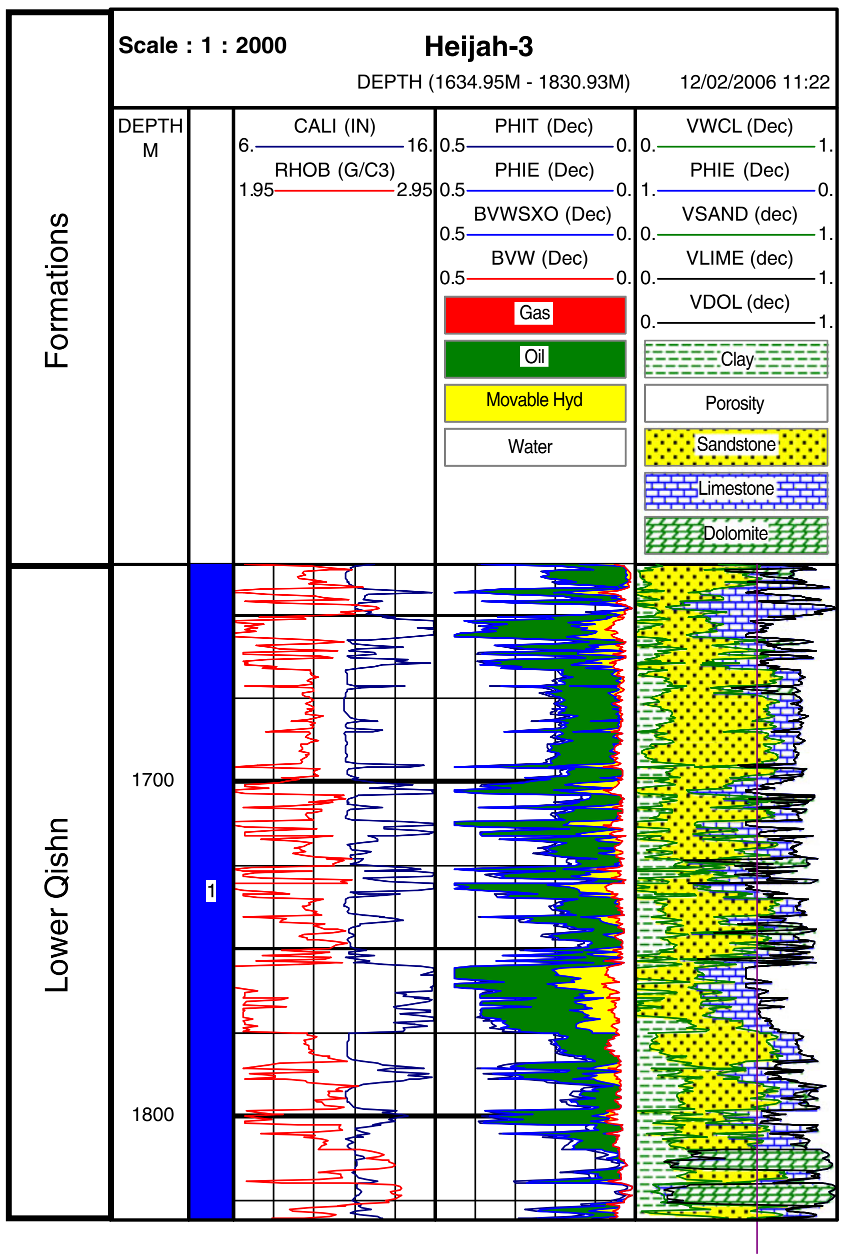

Fig. 6 Litho-saturation plot output showing log porosity derived from V_{sh} and S_w log of the Lower Qishn clastic Member in the study area

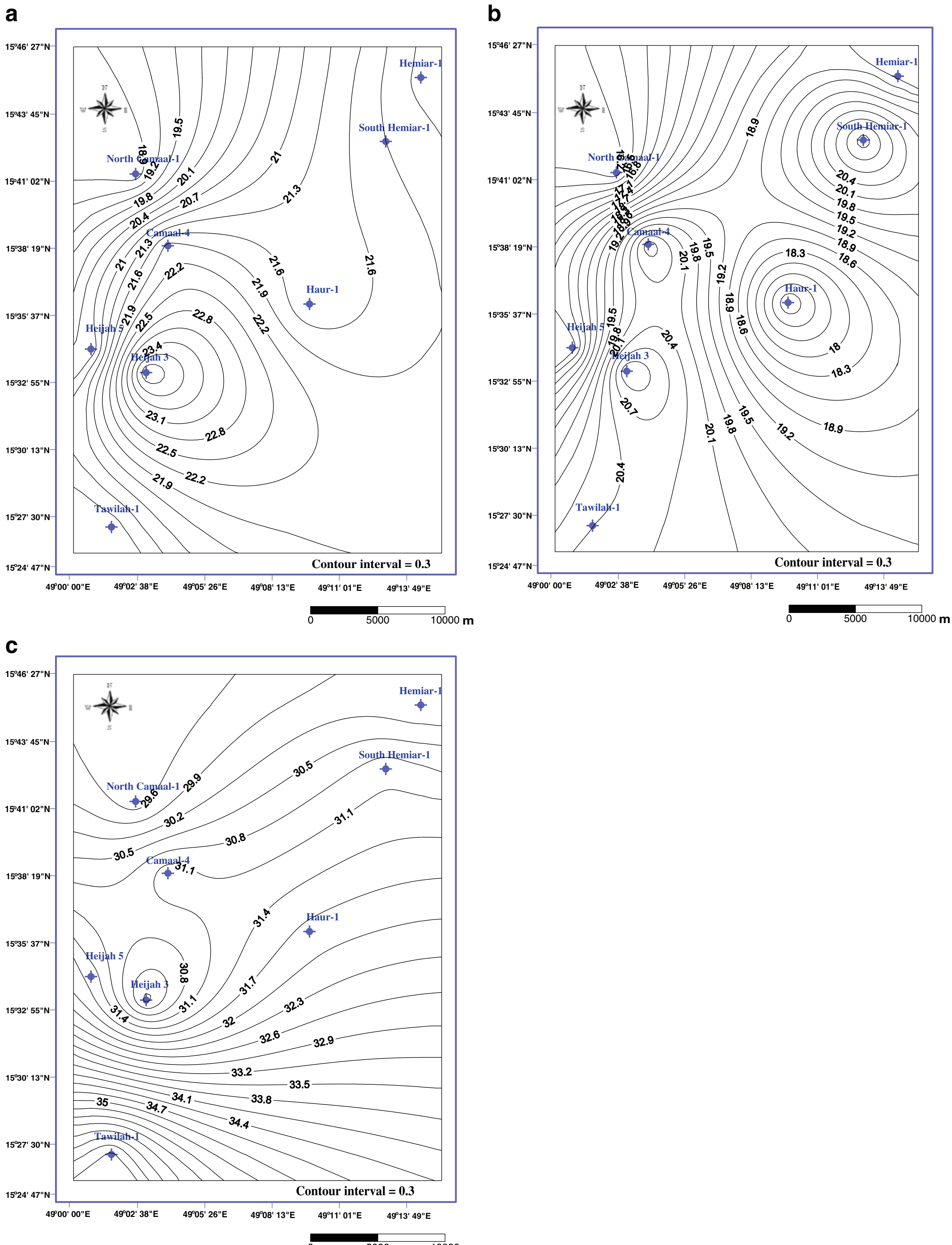

Fig. 7 **a** Total porosity distribution map of the Lower Qishn Member. **b** Effective porosity distribution map of the Lower Qishn Member. **c** Water saturation distribution map of the Lower Qishn Member

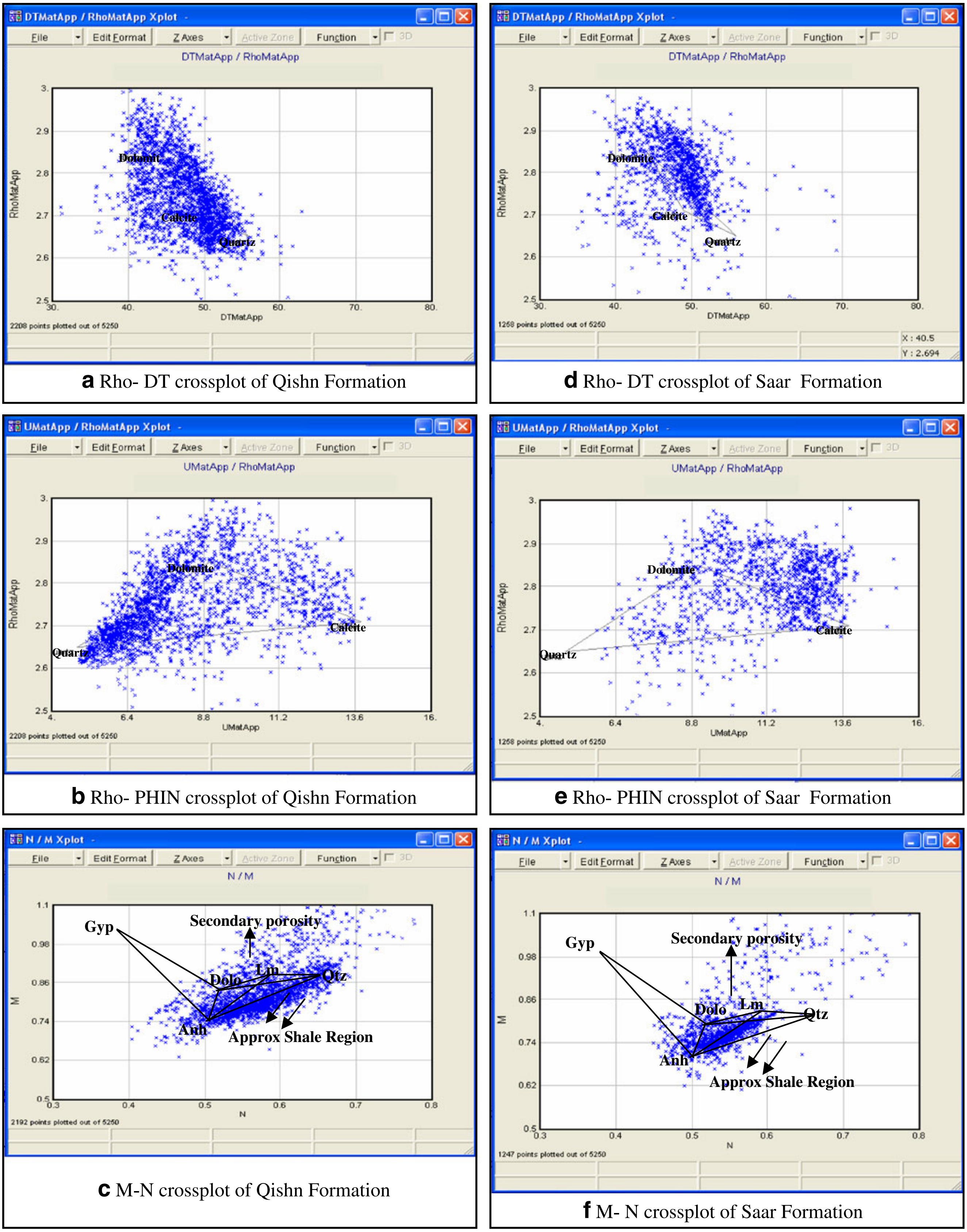

Fig. 8 Lithology and facies identification cross-plots for the Qishn and Saar formations. **a** Rho-DT cross-plot of Qishn Formation. **b** Rho-PHIN cross-plot of Qishn Formation. **c** M-N cross-plot of Qishn Formation

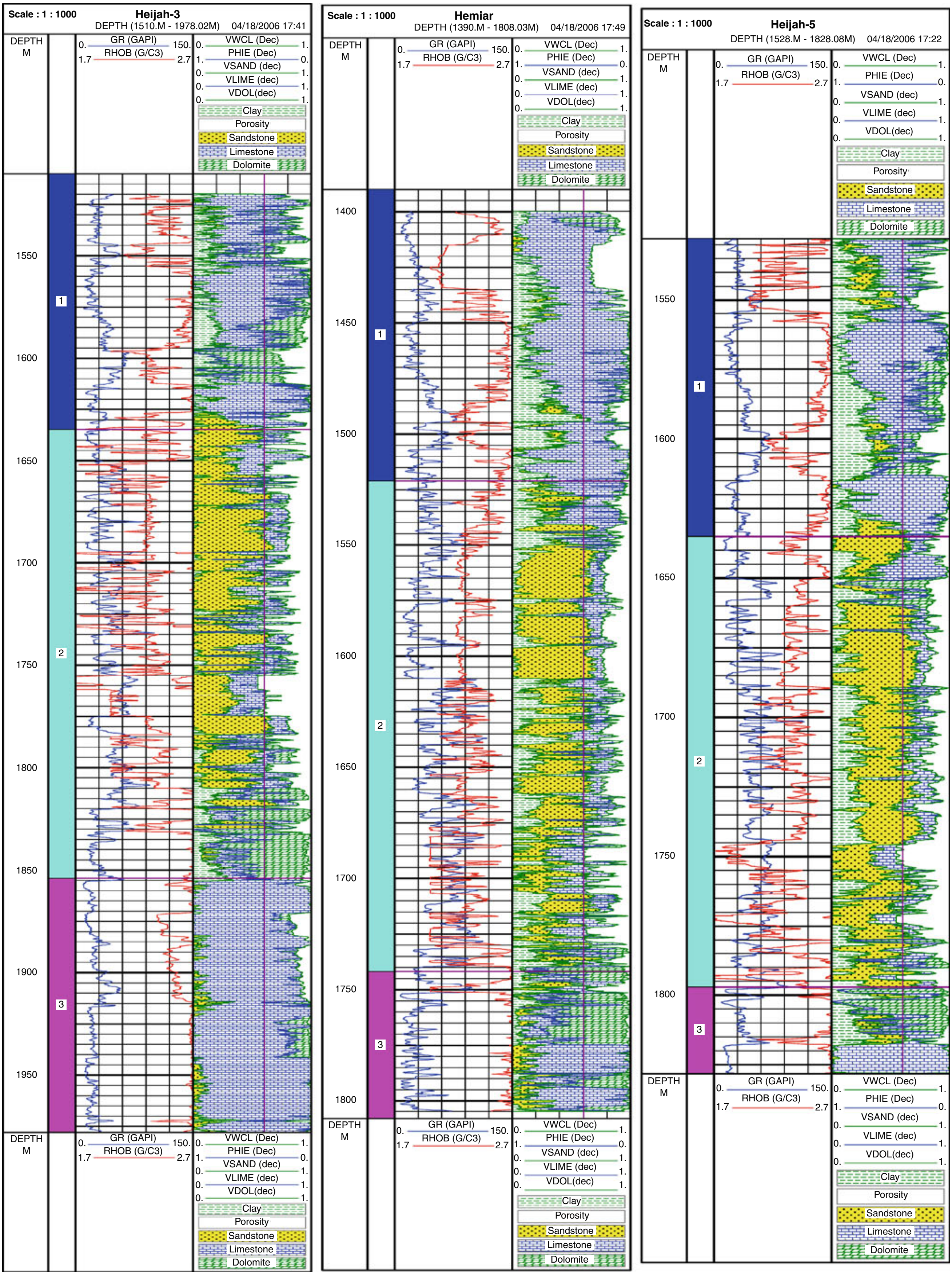
Scale : 1 : 1000
Heijah-3
DEPTH (1510.M - 1978.02M)
04/18/2006 17:41
DEPTH
M
GR (GAPI)
0.
150.
RHOB (G/C3)
1.7
2.7
VWCL (Dec)
PHIE (Dec)
VSAND (dec)
VLIME (dec)
VDOL(dec)
Clay
Porosity
Sandstone
Limestone
Dolomite
1550
1600
1650
1700
1750
1800
1850
1900
1950
1
2
3
Scale : 1 : 1000
Hemiar
DEPTH (1390.M - 1808.03M)
04/18/2006 17:49
1400
1450
1500
1550
1600
1650
1700
1750
1800
Scale : 1 : 1000
Heijah-5
DEPTH (1528.M - 1828.08M)
04/18/2006 17:22
1550
1600
1650
1700
1750
1800

◀**Fig. 9** Lithology of Heigah-3, Hemiar-1, and Heigah-5 well output from Interactive Petrophysics software

dolomite which is larger than that of the sandstone in the Lower Qishn Clastic rock unit. Thus, the points of limestone and dolomite locate in the left direction of the cross-plot. Finally, according to these cross-plots (Fig. 4a–d), it could be concluded that the lithology of this reservoir (Lower Qishn Clastic) is composed of sandstone with shale and carbonate. The sandstone content is generally high, as shown from the highest plotted points along the sandstone line.

Determination of the formation water resistivity (R_w)

In this work, the SP log is used to determine the R_w via Pc software, which is calculated for all the studied wells (Table 3).

Determination of formation porosity (φ)

In this work, the porosity can be determined from equations of the Inactive Petrophisecis software, which is calculated for all the studied wells for the studied formations. It could be concluded that the porosity of Lower Qishn Clastic in ranges from 19% to 24.9%, while the porosity of the Saar Formation ranges from 6% to 19.7%.

Determination of fluid saturation

The determination of fluid saturation is very important to complete the deduced petrophysical parameters of the studied reservoir rock units. The hydrocarbon saturations for the studied rock units are calculated depending on water saturation (S_w). The hydrocarbon saturation can be calculated by the following relation:

$$S_h = 1 - S_w.$$

It can be concluded that the water saturation for Lower Qishn Clastic ranges from 30% to 38% and for Saar Formation from 53% to 80% (Table 3).

Hydrocarbon potentiality

Evaluation of the oil potential of the reservoir rocks in the study area is based on the results of well logging

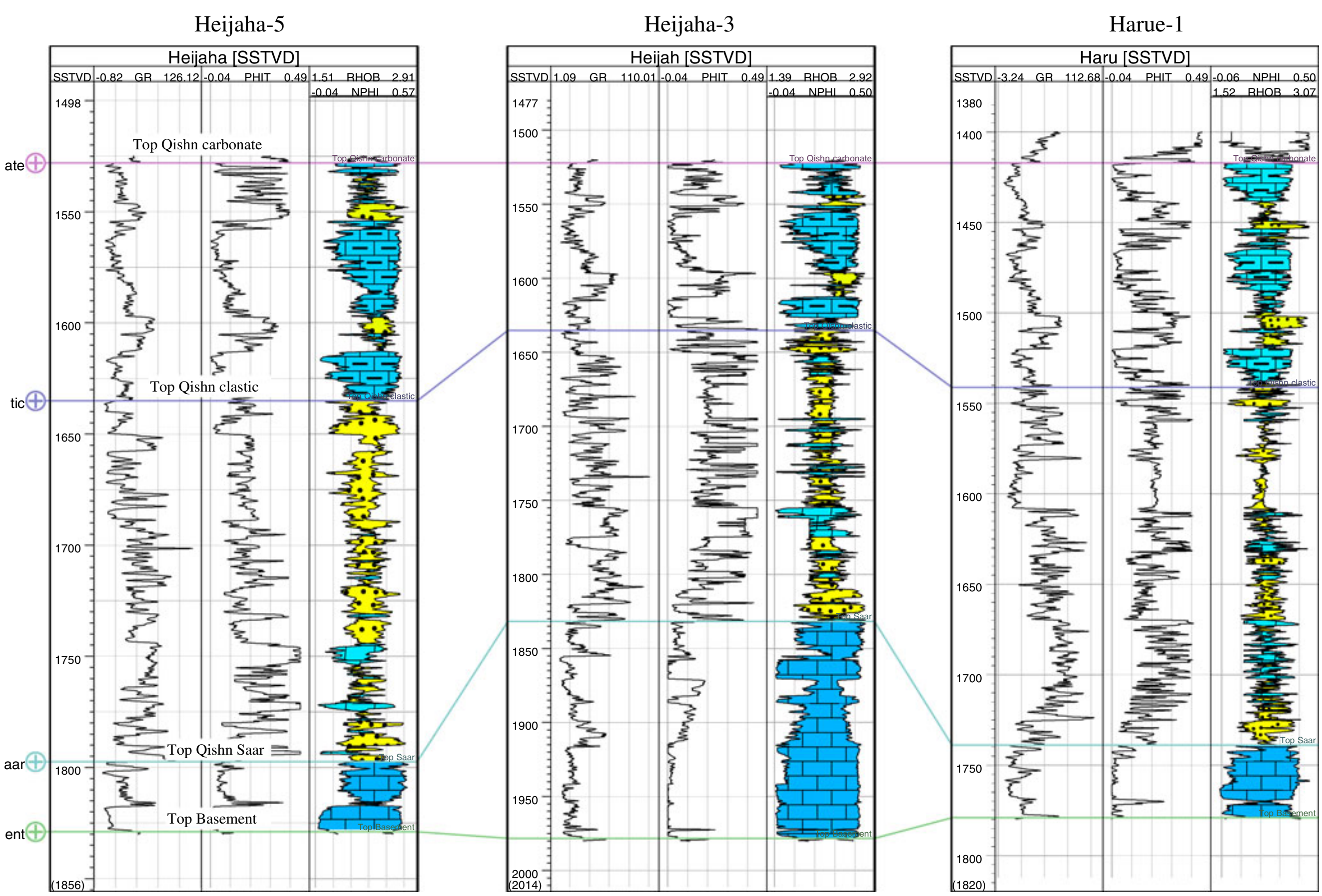

Fig. 10 Correlation and lithology of Heijaha-5, Heijaha-3, and Harue-1 well output from Interactive Petrophysics software

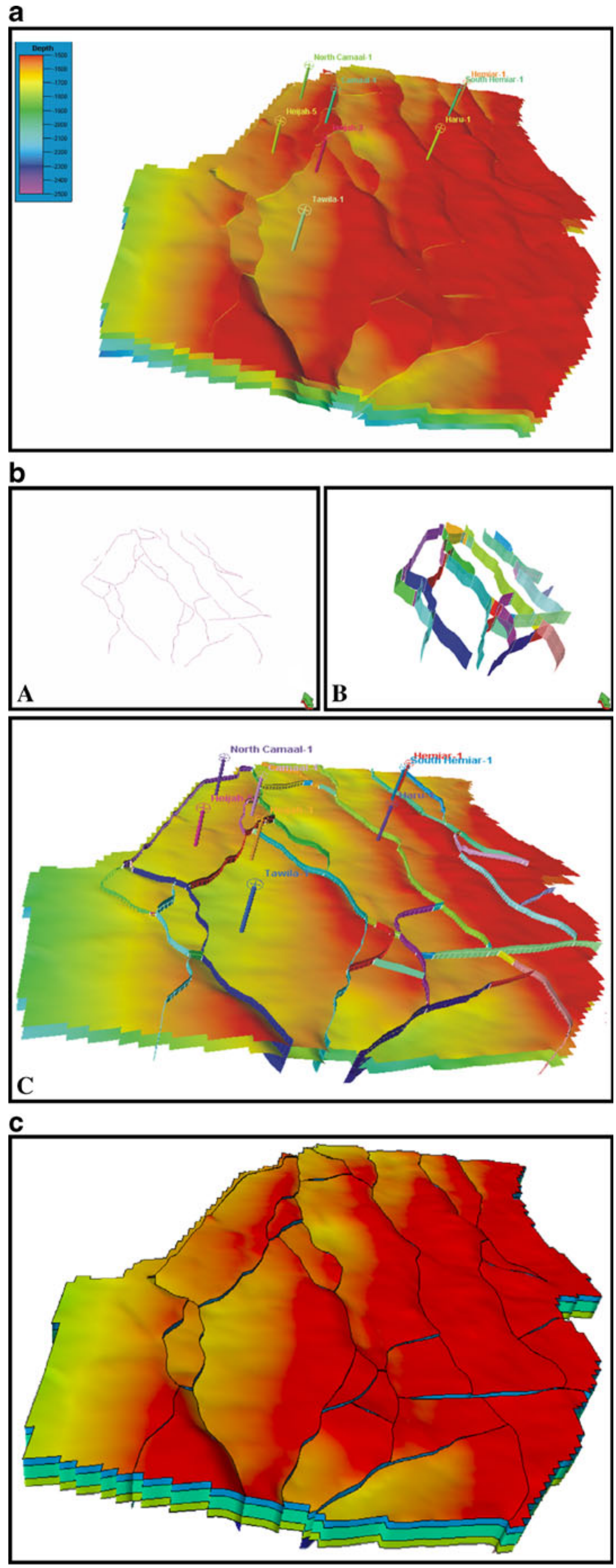

Fig. 11 **a** Structural model of the Masila area showing the major fault and selected horizons: pre-fault top of basement (*blue surface*); syn-fault tops of the Upper Qishn and Lower Qishn members and Saar Formation (*red*, *yellow*, and *green surfaces*, respectively). **b** Fault model showing fault outline system (*A*), fault surfaces (*B*), and surface appended of the horizons (*C*) in the Masila oil field. **c** 3D structural model includes faults, stratigraphy, and geometry of the reservoirs in the study area

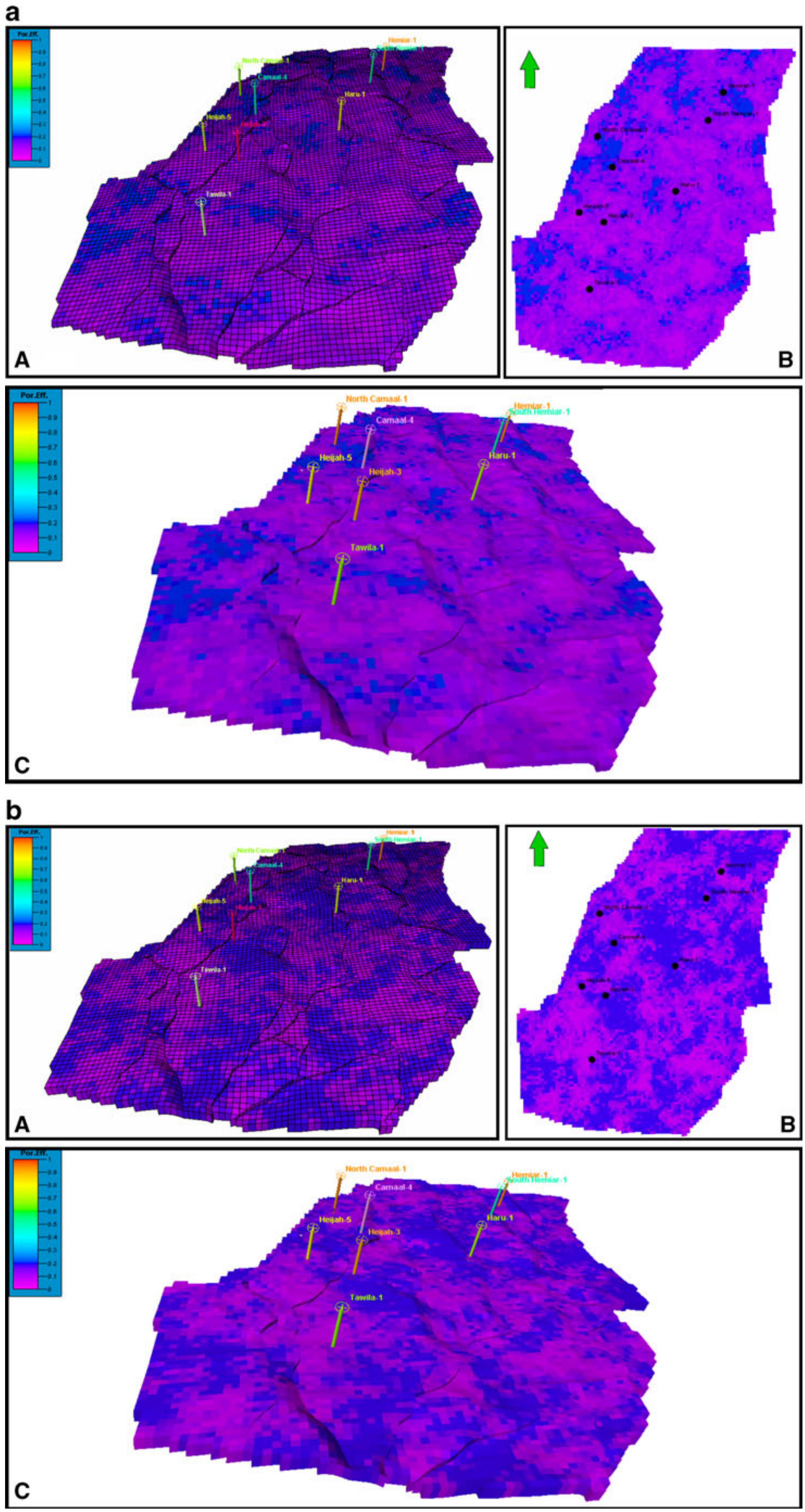

Fig. 12 **a** Porosity model output: 3D gridding model (*A*), horizontal slice sequential Gaussian simulation (*B*), color-coded according to porosity of the Upper Qishn Member (*C*)

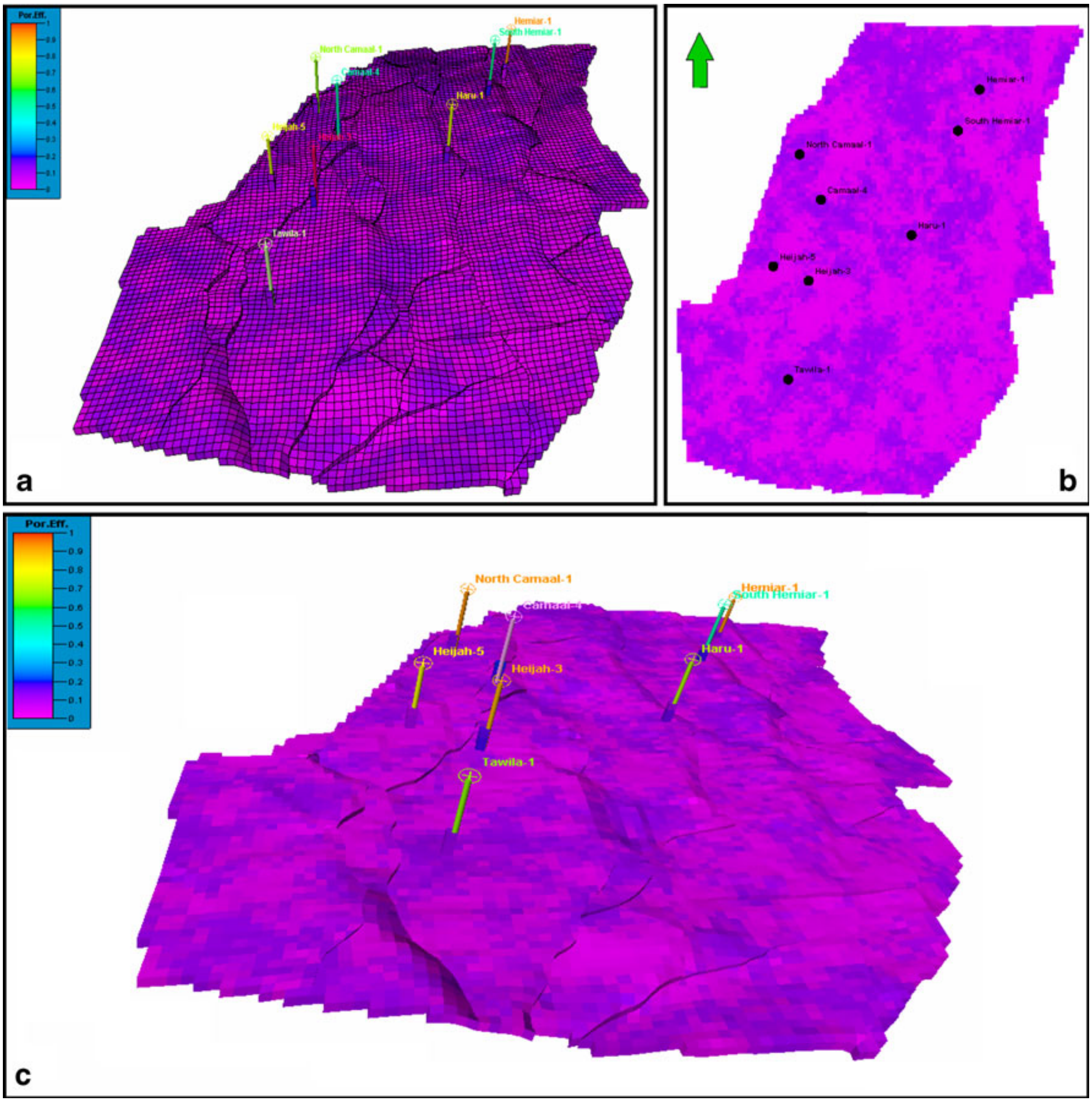

Fig. 13 Porosity model output: 3D gridding model (**a**), horizontal slice sequential Gaussian simulation (**b**), color-coded according to porosity of the Saar Formation (**c**)

analysis for the studied wells. These analyses include vertical petrophysical distribution cross-plots of the analyzed data in each well and the horizontal isoparametric configuration maps. The vertical distribution, in a form of litho-saturation cross-plots (volumetric analysis), shows irregular changes in lithology and water and hydrocarbon contents (Fig. 6). The lateral isoparametric maps show the petrophysical parameter configuration in the form of water and hydrocarbon saturations, total porosity, and effective porosity distribution (Fig. 7a–c).

The total porosity of the Lower Qishn Clastic (Fig. 7a) decreases from the central-western part toward the northwestern, southwestern, and eastern parts of the study area. The effective porosity (Fig. 7b) decreases from the central-southern part toward the east and northwest and increases at the northeastern part of the study area. Meanwhile, the water saturation map of the Lower Qishn Clastic shows a decrease from the central-western part toward the east, northeastern, and southwestern parts of the study area (Fig. 7c).

Fig. 14 **a** Permeability model output: 3D gridding model (*A*), horizontal slice sequential Gaussian simulation (*B*), color-coded according to permeability of the Upper Qishn Member (*C*). **b** Permeability model output: 3D gridding model (*A*), horizontal slice sequential Gaussian simulation (*B*), color-coded according to permeability of the Lower Qishn Member (*C*) ▶

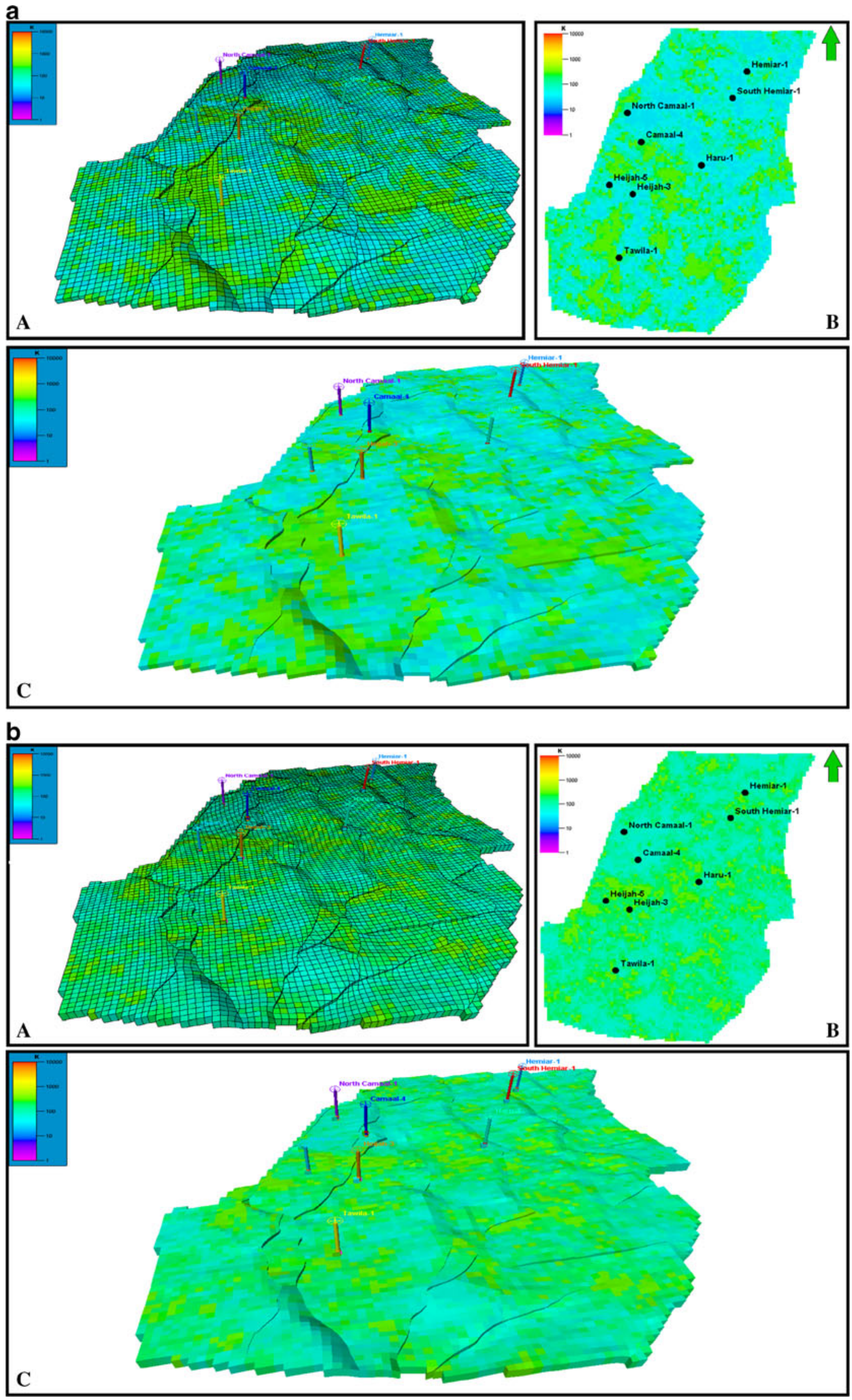
a
K
10000
1000
100
10
1
Hemiar-1
South Hemiar-1
North Camaal-1
Camaal-4
Haru-1
Heijah-5
Heijah-3
Tawila-1
A
B
C
b
A
B
C

Determination of lithology

Cross-plot technique, combined with the different well log parameters, was applied here to identify lithology types and define the mineralogical associations of each lithotype. A number of cross-plots (ρb vs. Φ_N, GR vs. ρb, ρb vs. ΔT) for both Qishn and Saar formations are given in Fig. 8a–f. It could be concluded that the lithology of Lower Qishn Clastic Member is composed mainly of sandstones with dolomite and limestone, while the Upper Qishn Carbonate Member consists of carbonates (limestone and dolomite) with shale and has low sandstone content. The lithology of the Saar Formation is consists mainly of carbonate (limestone and dolomite) with shale and sandstones (Figs. 8a–f, 9, and 10).

3D geomodeling

3D geological modeling

The stratigraphy of the studied reservoir can be summarized as follows, from top to bottom:

(a) Upper Qishn Member (red surface)
(b) Lower Qishn Member (green surface)
(c) Saar Formation (yellow surface)

The top and base structure maps were digitized and transformed into surfaces (Fig. 11a). The main geological feature in this field is a system of faults (Fig. 11a, b) that divides the field into eastern and western sections. The fault system, as well as other smaller faults, was modeled as vertical fault surfaces (Fig. 11b, c).

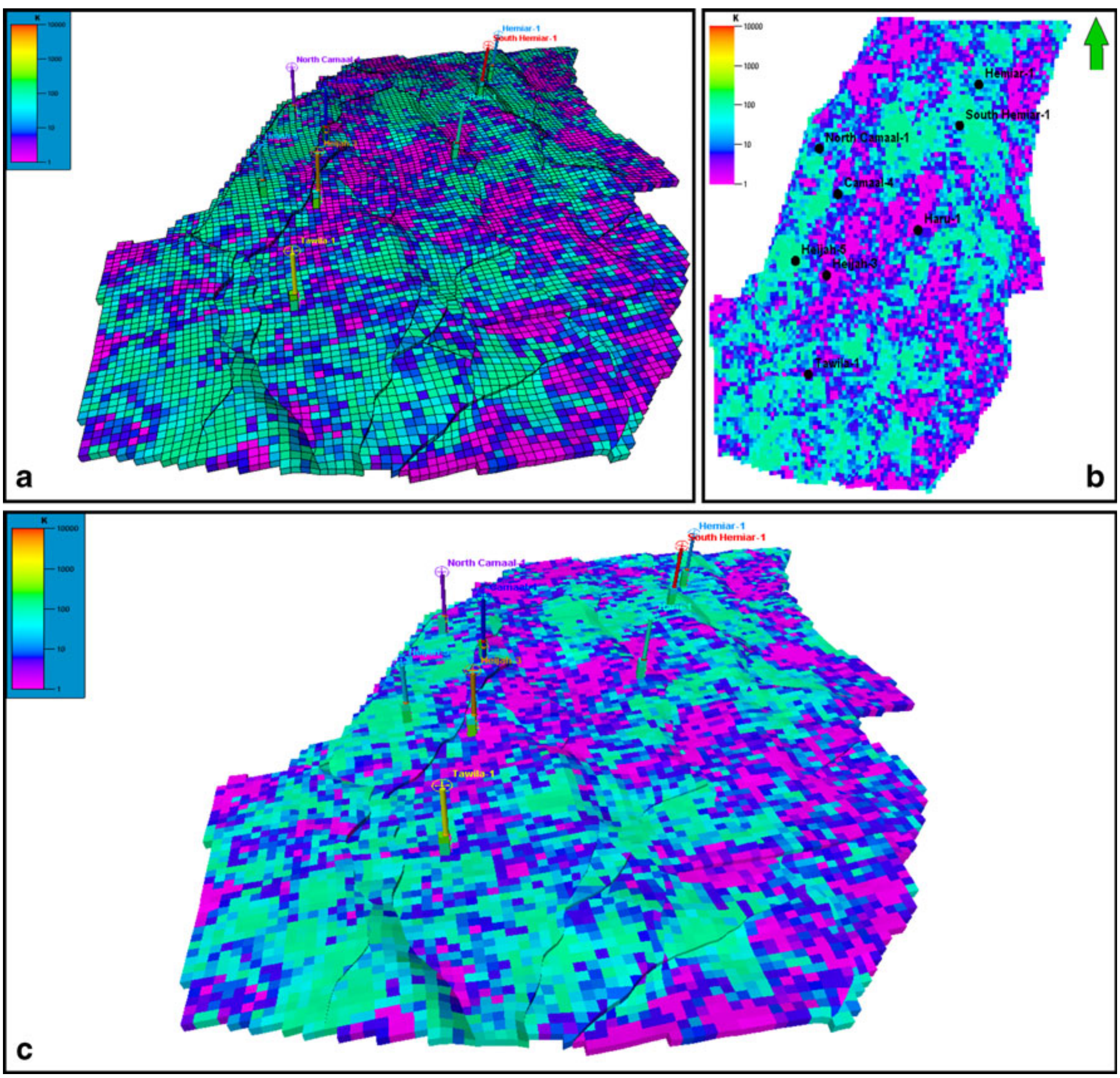

Fig. 15 Permeability model output: 3D gridding model (**a**), horizontal slice sequential Gaussian simulation (**b**), color-coded according to permeability of the Saar Formation (**c**)

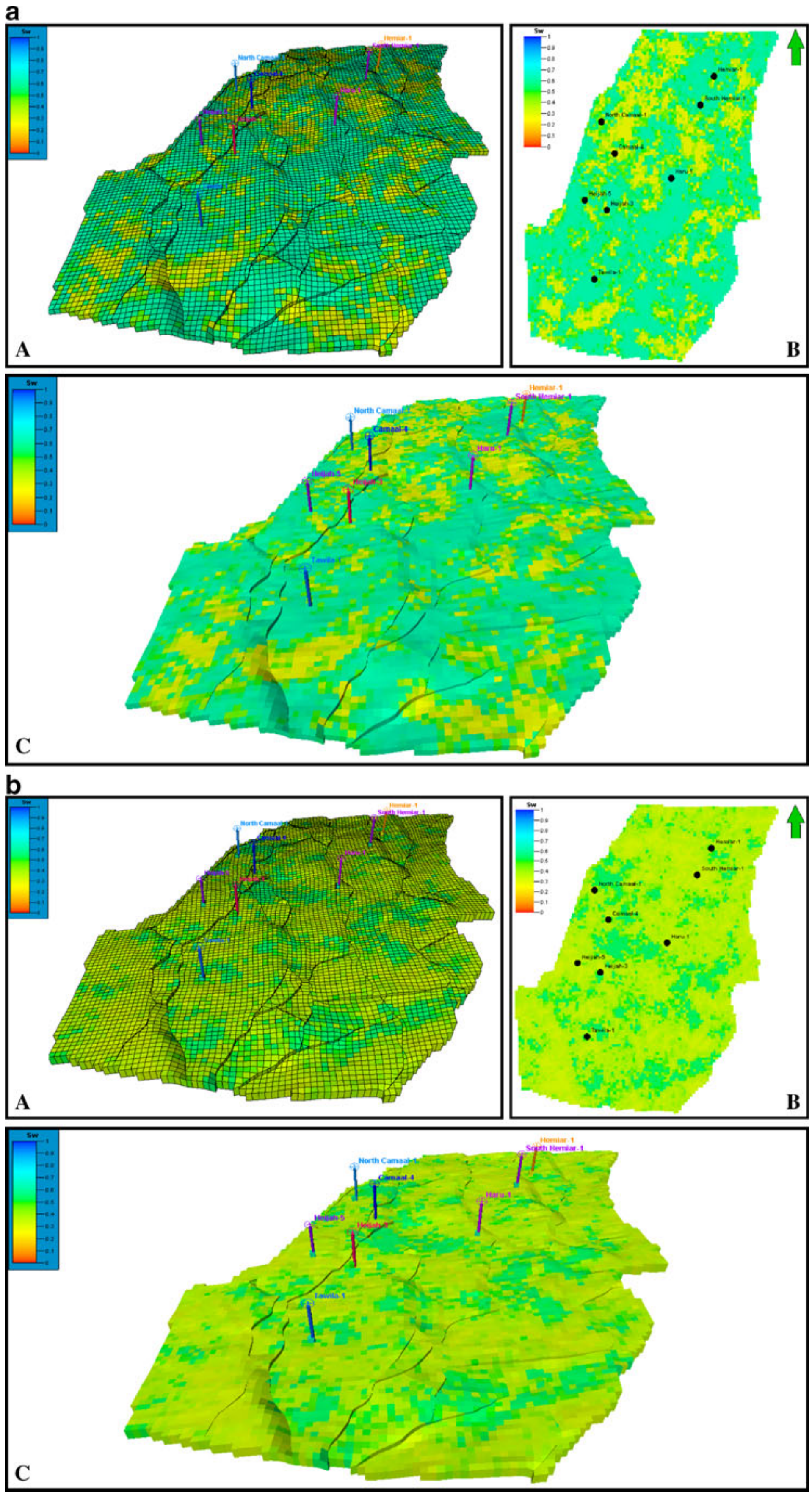

Fig. 16 **a** Water saturation model output: 3D gridding model (*A*), horizontal slice sequential Gaussian simulation (*B*), color-coded according to water saturation of the Upper Qishn Member (*C*). **b** Water saturation model output: 3D gridding model (*A*), horizontal slice sequential Gaussian simulation (*B*), color-coded according water saturation of the Lower Qishn Member (*C*)

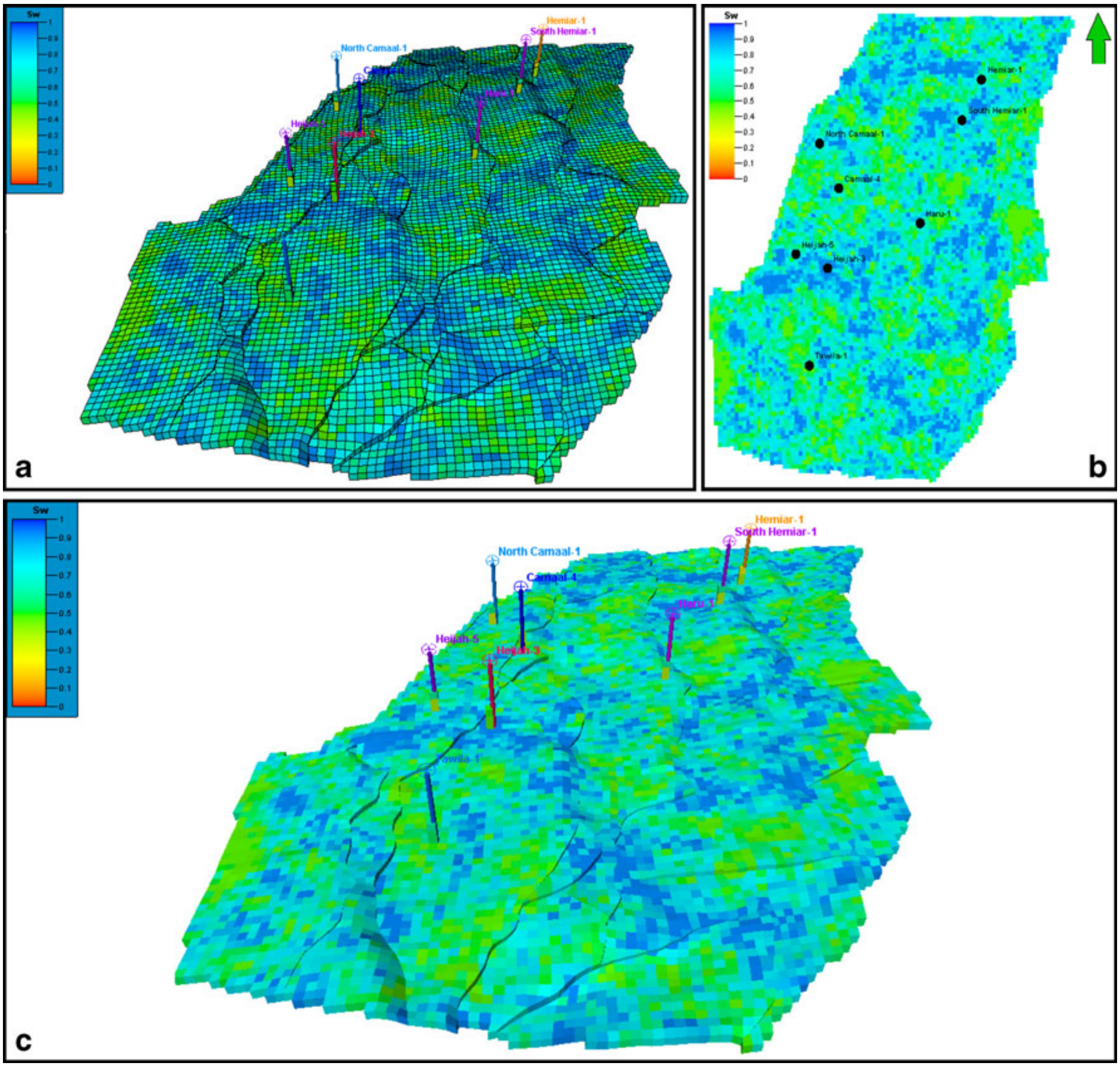

Fig. 17 Water saturation model output: 3D gridding model (**a**), horizontal slice sequential Gaussian simulation (**b**), color-coded according to water saturation of the Saar Formation (**c**)

Petrophysical model

Figures 12a, b and 13 show geological models for the porosity, permeability, and water saturation distribution created by SGS in the study area. Those models reflect that the porosity values for the Upper Qishn Member range from 9.5% to 14.5%. The porosity model of the Lower Qishn Member (Fig. 12b) reflects porosity values that do not exceed 21.5%. However, the porosity model of the Saar Formation (Fig. 13) shows that the porosity values range from 3% to 12%.

In the studied reservoir, the permeability model of the Upper Qishn Member (Fig. 14a) shows that the permeability values range from 43 to 155 md, while the permeability model of the Lower Qishn Member (Fig. 14b) illustrates that the permeability values range from 100 to 380 md. The permeability model of the Saar Formation (Fig. 15) shows that the permeability values range from 1 to 65 md.

The water saturation model of the Upper Qishn Member (Fig. 16a) shows that the water saturation values range from 57% to 62%. The water saturation model of the Lower Qishn Member (Fig. 16b) illustrates that the water saturation values range from 29% to 37%. The water saturation model of the Saar Formation (Fig. 17) shows that the water saturation values range from 52% to 76%.

Fig. 18 **a** Facies model output: 3D gridding model (*A*), horizontal slice sequential indicator simulation (*B*), color-coded according to facies of the Upper Qishn Member (*C*). **b** Facies model output: 3D gridding model (*A*), horizontal slice sequential indicator simulation (*B*), color-coded according to facies of the Lower Qishn Member (*C*) ▶

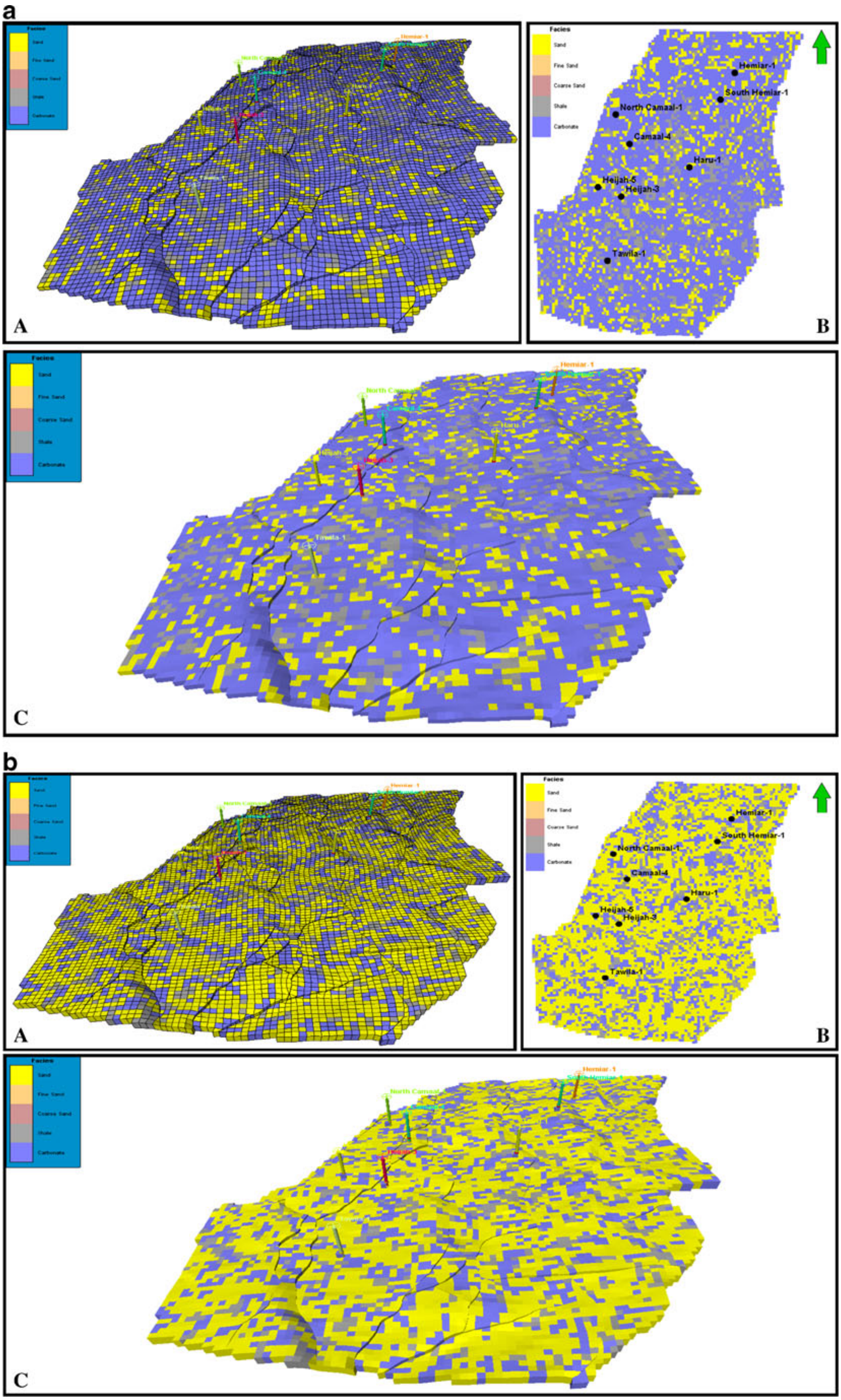
a
Facies
Sand
Fine Sand
Coarse Sand
Shale
Carbonate
Hemiar-1
South Hemiar-1
North Camaal-1
Camaal-4
Haru-1
Heijah-5
Heijah-3
Tawila-1
A
B
C
b
A
B
C

Facies model

The facies model of the Upper Qishn Member (Figs. 18a, b and 19) shows that it is composed mainly of carbonate with shale and a few of sandstones. The facies model at the Lower Qishn Member shows that it is composed of sandstone with shale and carbonates. Meanwhile, the facies model of the Saar Formation shows that it is composed mainly of carbonates with shale and sandstone.

Reservoir flow model

The geological model was converted into a flow model with 750,000 (500×500×3) grid blocks. This flow model will be used to evaluate the productive potential of the Lower Cretaceous reservoirs (Fig. 20). Figure 21 shows a 3D geological model for the studied Lower Cretaceous Masila reservoirs.

Summary and conclusions

1. In the fields of the Masila block, the Early Cretaceous marine Qishn Formation provides both the reservoir sandstone and an overlying sealing tight limestone unit.
2. The largest hydrocarbon volumes are reservoired in sands of the Qishn Formation sands of Barremian–Aptian age that have produced considerable rates of oil with little dissolved gas.
3. The Qishn Formation comprises shallow shelf to fluvio-deltaic sandstones in central and western Yemen and is

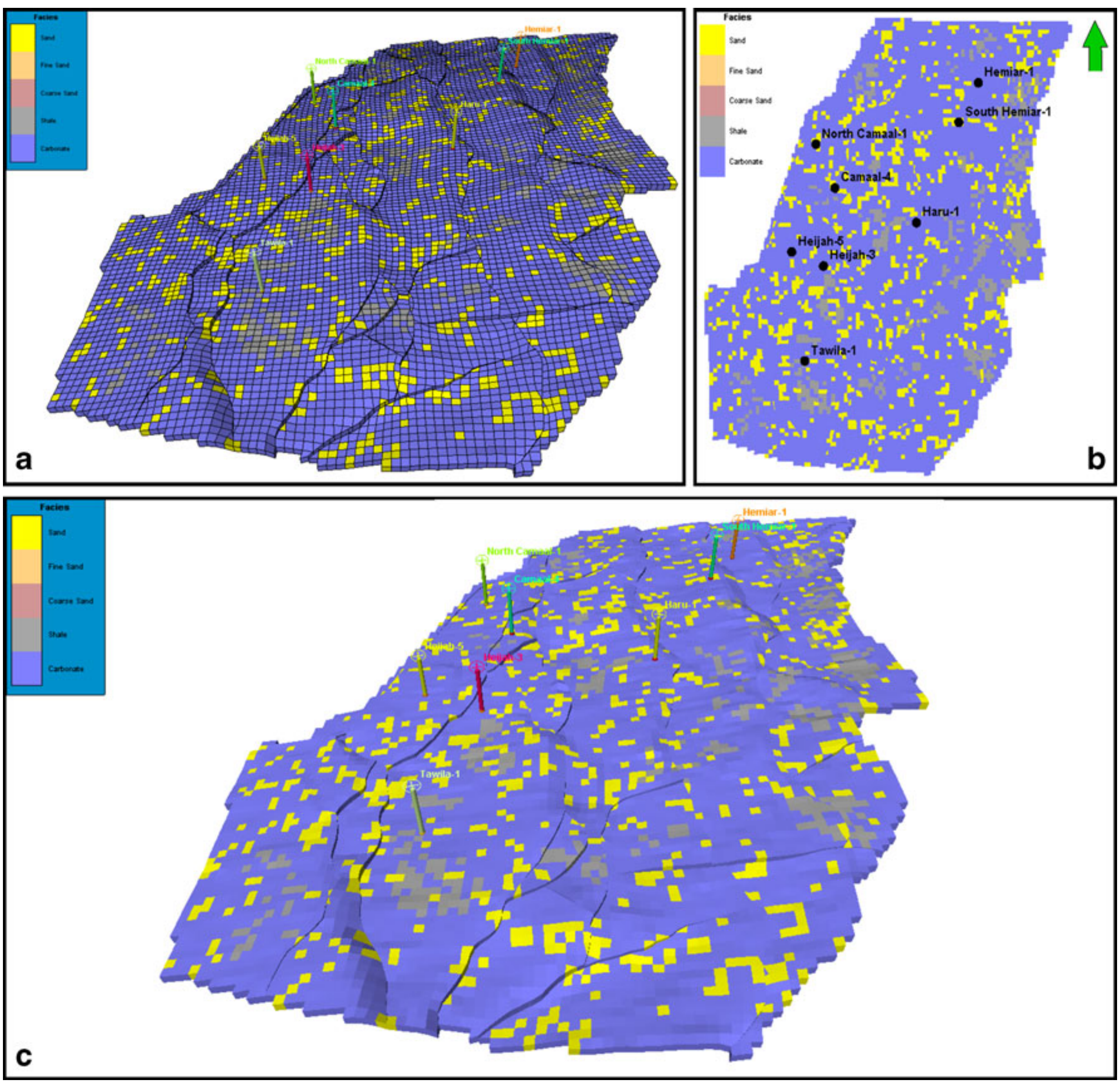

Fig. 19 Facies model output: 3D gridding model (**a**), horizontal slice sequential indicator simulation (**b**), color-coded according to facies of the Saar Formation (**c**)

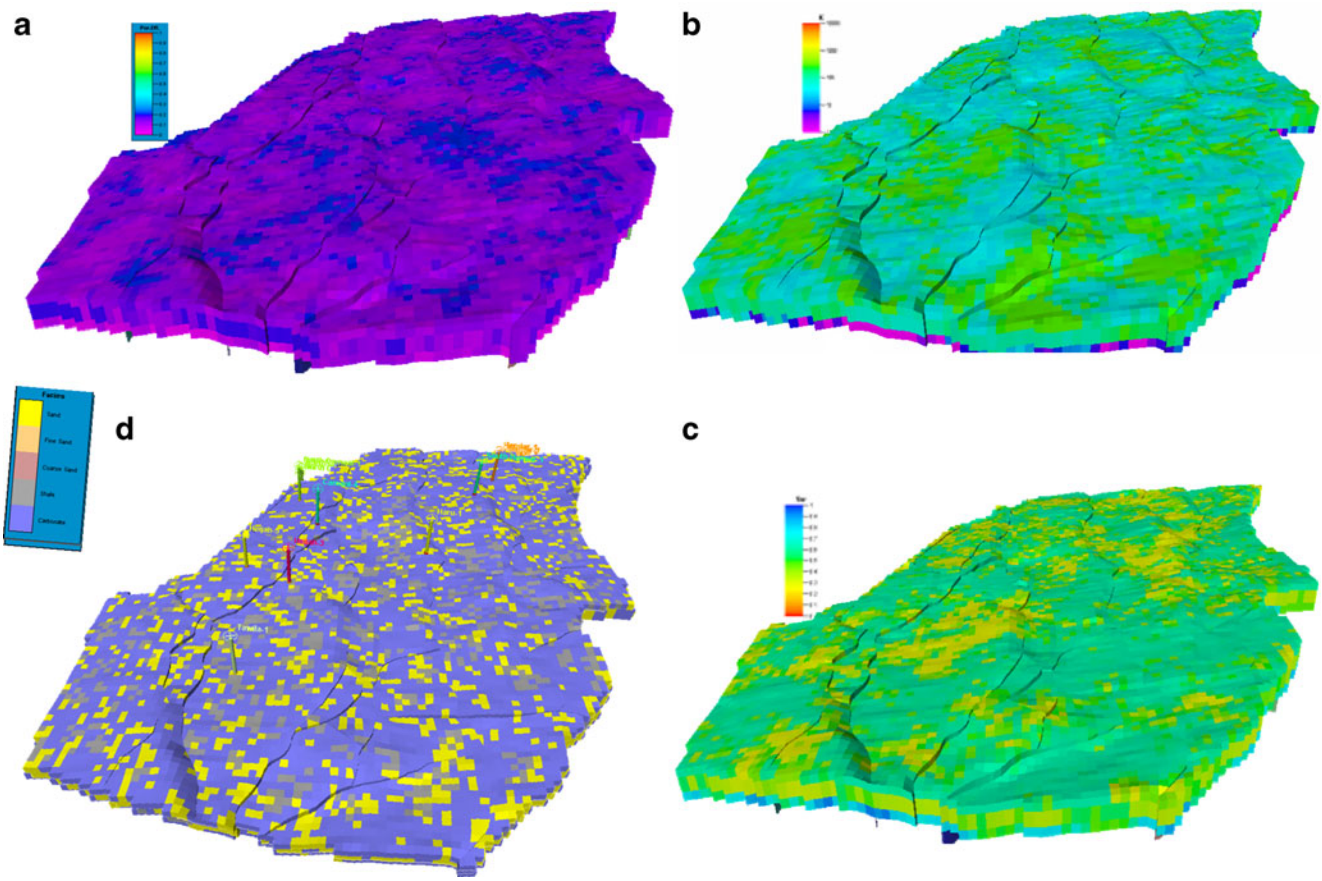

Fig. 20 Property modeling of Lower Cretaceous Reservoirs in Masila oil field: porosity model (**a**), permeability model (**b**), water saturation model (**c**), and facies model (**d**)

likely to be equivalent to the lower fluviatile sandstones of the Tawilah Group of western Yemen, and to the east, it becomes more carbonate-rich and passes into the purer carbonate facies of the Mahra Group.

4. The porosity analyses illustrated that the total porosity ranges from 18% to 24.3% while the effective porosity ranges from 25% to 18%. The permeability of this reservoir ranges from 375 to 103 md. The water saturation values range from 29% to 37%, whereas the hydrocarbon saturation has matched with the water saturation in a reverse relationship. The hydrocarbon occurrence decreases where the water saturation increases.

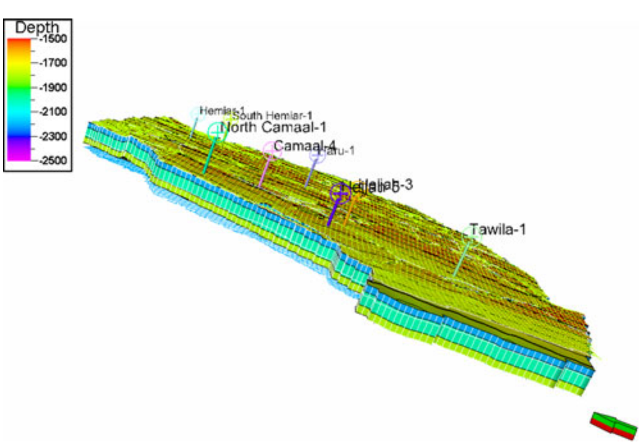

Fig. 21 3D geological model for Lower Cretaceous Masila reservoir

5. The lithological identification of the investigated reservoir indicates that the main lithology is made up of sandstone with shale and carbonates. The utility of cross-plots illustrated that the Qishn Formation is composed mainly of sandstone with limestone and dolomite, and Saar Formation is composed mainly of limestone and dolomite with shale and low content of sandstone.
6. The petrophysical parameters refer to high hydrocarbon saturation with many pay zones in the studied reservoir. Hydrocarbon saturation of the Qishn Formation is higher than that of the Saar Formation.
7. Reservoir properties of well log analysis were augmented by similarly detailed seismic and stratigraphic correlations and then integrated together in a 3D geological model. The integration of such inputs enhances considerably not only the static reservoir description but also the consistency of the future

reservoir model, which will better reproduce the observed field performance and facilitate at a later stage the production history matching process.

References

Beydoun ZR (1964) The stratigraphy and structure of the Eastern Aden protectorate. Overseas Geol Miner Resour, Suppl Ser, Bull Suppl 5. HMSO London, 107 pp

Beydoun ZR (1966) Eastern Aden protectorate and part of Dhufar. In: Geology of the Arabian Peninsula. USGS Professional Paper 560H, Washington, DC, 49 pp

Beydoun ZR, Greenwood JEGW (1968) Aden protectorate and Dhufar. In: Dubertret L (ed) Lexique Stratigraphique International, vol. III. Asie fasc

Beydoun ZR, As-Saruri MAL, El-Nakhal H, Al-Ganad IN, Baraba RS, Nani ASO, Al-Aawah MH (1998) International lexicon of stratigraphy, Volume III, Republic of Yemen, Second Edition: International Union of Geological Sciences and Ministry of Oil and Mineral Resources, Republic of Yemen Publication 34, 245 p

Canadian Oxy Company (2003) Yemen (unpublished report)

Greenwood JEGW (1967) Photogeological map of Western Aden Protectorate, scale 1:250,000. D.O.S. (Geol.) 1159A

Greenwood JEGW, Bleackley D (1967) Aden protectorate. In: Geology of the Arabian Peninsula. USGS Professional Paper 560-C. Washington, DC, 96 pp

Holden A, Kerr HM (1997) A subsurface lithostratigraphic division of the Hauterivian to Aptian, Furt (informal) and Qishn formations, Yemen. Mar Petrol Geol 14:631–642

Khalil M, Naji HS (2010) 3D structural geomodeling and oil occurrence of the Lower Cretaceous successions, Masila Oilfield, Yemen. Journal of Geological Society of India (in press)

Mills SJ (1992) Oil discoveries in the Hadramaut: how Canadian Oxy scored in Yemen. Oil Gas J Spec 9:49–52

Naji HS (2010) Reservoir properties of Lower Cretaceous Qishn and Saar formations from well logs analyses of Masila Region, Yemen. JKAU: Earth Sci 21(2) (in press)

Naji HS, Khalil M (2010) Hydrocarbon potentialities and reservoir characterization of Lower Cretaceous successions of Masila Oil field, Yemen. JKAU: Earth Sci (in press)

Naji HS, Hakimi H, Khalil M, Sharief FA (2010a) Stratigraphy deposition and structural framework of the Cretaceous and 3D geological model of the Lower Cretaceous reservoirs, Masila Oil Field, Yemen. Arab J Geosci 3(3):221–248

Naji HS, Sharief FA, Khalil M (2010b) Sedimentology and quantitative well logs petrophysical parameters, Lower Qishn Clastic reservoir, Masila Oilfield, Yemen. JKAU: Earth Sci 21(1):53–77

Rojstaczer S, Ingebristen E, Hayb DO (2008) Permeability of continental crust influenced by internal and external forcing. Geofluids 8:128–139